Iranian Journal of Chemistry and Chemical Engineering (IJCCE)

Effects of transient consecutive cyclic injection-suction of a fluid on the interfacial dynamics during a radial immiscible fluid-fluid displacement inside a Hele-Shaw cell

Majid Ahmadlouydarab*, Mohammad Kangari[1]

[1] Faculty of Chemical & Petroleum Engineering, University of Tabriz, Iran

*Corresponding author: mahmadlouydarab@tabrizu.ac.ir

Abstract:

In current study, the inabilities resulting from the interaction of two Newtonian immiscible fluids, including water and base oil, during transient consecutive injection-suction in a Hele-Shaw cell, was studied. For injection-suction purposes, base oils with viscosities of 150, 920 and 1506 cP were used. The highest continuous flow rates for three techniques including pseudo-sinusoidal, percussive time-dependent, and constant-flow rate were 10, 20, and 30 ml/min, respectively. The volume of fluid injected or extracted remained consistent across all three methods. The injection-suction process was repeated for five full cycles to analyze the impact of frequency on the outcome. The primary goal was to study how to eliminate interfacial instabilities and restore the circular shape of the fluid-fluid interface after each cycle. It was found that the percussive and constant-flow rate methods were unable to achieve this objective. Results showed that the growth rate of interfacial instabilities was slower with the pseudo-sinusoidal method compared to the other methods. Increasing the flow rate in the constant-flow rate method resulted in more oil packets being created. The pseudo-sinusoidal method did not show instabilities like water droplets, fingers, or oil packets, unlike the constant-flow rate and percussive methods. Overall, the pseudo-sinusoidal method was found to be the most suitable for restoring the fluid-fluid interface to its original stable state. However, increasing the number of cycles could lead to more instabilities, making it harder to return to the initial stable interface.

Keywords: *Immiscible fluid-fluid radial displacement; Hele-Shaw cell; Transient; Consecutive cyclic; consecutive injection-suction; viscous fingering*

1. INTRODUCTION

The movement of one fluid by another can result in either stable or unstable displacement. Unstable displacement can lead to the penetration of fingers of one fluid into another. For example, in horizontal flow, a lower viscosity fluid displacing a higher viscosity fluid can result in the formation of fingers. The Hele-Shaw cell is a commonly used device for studying fluid displacement in a uniform porous medium. There are different types of Hele-Shaw cells used in laboratories to run experiments. It is common to using this device instead of real porous media as it allows for similar flow characteristics and aids in experimental and modeling processes. Figure (1) illustrates a schematic of the Hell-Shaw cell. In that figure, "r_b" represents the base radius or minimum radius and "r" indicates the maximum radius of the fingers.

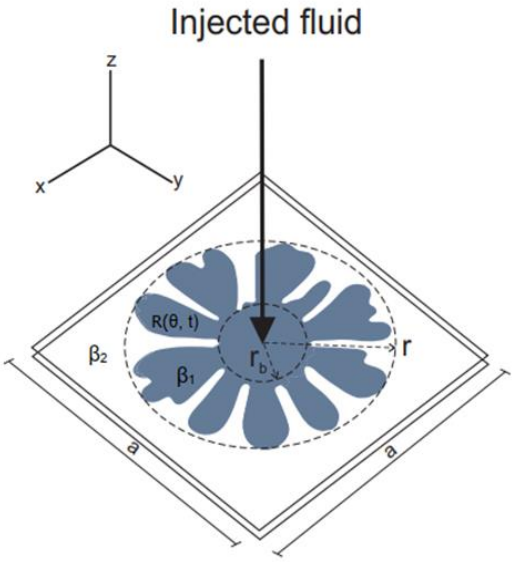

Figure 1: Schematic of the 3D Hele-Shaw cell with some parameters including the base (r_b) and the maximum (r) radii.

The interfacial instabilities present at fluid-fluid interface were first studied in an experimental study by Hill [1], and then by Slobod and Caudlel [2] in 1952. However, the interfacial dynamics analysis was first presented by Saffman and Taylor [3] in 1958. Various characteristics of two fluids displacement inside the Hele-Shaw cell have been investigated, including solid substrate stress [4, 5], non-Newtonian fluid interfacial morphology [6, 7], surface smoothness [4], plates anisotropy [8, 9], fluids viscosity ratio [10], plates spacing [11], densities and viscosities distribution [12], and gravitational forces [13]. Literature shows that, lots of researches on the fluid-fluid interfacial instability have been done by Homsy, Yortsos, and McCloud & Maher [14-16]. In 1968, Bataille, and later in 1981 Paterson studied the key important parameters effects on the increased instability during the early stages of immiscible fluid-fluid displacement [17, 18]. Later, in 1995, Cardoso and Woods studied the impacts of surface stress demonstrating the direct correlation between injection radius and the interfacial stability [19]. In another experimental study in 1995, Hornof and Baig investigated the impact of oil viscosity [20]. They injected water from the corner of the Hale-Shaw cell. Authors showed that the oil recovery increased as the mobility ratio decreased, and adding the reactants to oil and water led to an increment in oil recovery factor. In

most industrial applications the injection processes are time-dependent, while in most of the researches constant injection flow rates have been considered for fluid-fluid displacement. Pisarenko and Gland examined impacts of oscillation on injected air pressure on the fingering instability [21]. Utilizing air to displace oil in the Hele-Shaw cell, they concluded that pressure fluctuations resulted in a reduction of finger development. In a separate study, Brailovsky, carried out numerical simulations on radial displacement of fluids in the Hele-Shaw cell, revealing that a prolonged interruption in the injection process led to interfacial stability, reduction and contraction of the fingers shape [22]. In 2010, Dias and colleagues employed linear stability analysis to investigate interfacial displacements inside the Hele-Shaw cell. They suggested the patch injection method as a means to minimize interfacial instability [23]. In yet another study, once more, Dias and colleagues demonstrated in 2010 that altering the injection rate by $t^{-\frac{1}{3}}$, could have a significant impact on reducing finger bifurcation during nonlinear injection [24]. In 2011, Reis and Miranda utilized linear stability analysis to manage the viscose fingering instability in radial injection into the Hele-Shaw cell [25]. Furthermore, Dias highlighted that the immiscible fluid-fluid radial displacement with constant injection rates method has the potential to minimize instability more effectively than other fluid injection methods [26]. Later in 2013, a linear injection method introduced by Dias validated that constant injection flow rates result in reduced instability in immiscible fluid-fluid displacements [27]. In the model developed by Dias and colleagues, it is feasible to achieve the stable morphology in the radial injection method in the Hele-Shaw cell by regulating and selecting specific fixed injection rates. Yuan and Azaiez studied the miscible fluid-fluid displacement during cyclic time-dependent fluid injection in 2014 and 2015 [28, 29]. Their results revealed that stable constant injection can transform into instability when converted to time-dependent injection, leading to complicating fingers and increased reactivity due to the mixing of the two fluids. In another study, Yuan and Azaiez findings indicated that the level of instability can differ based on the injection cycle period and its range [29]. In 2015, Chen introduced a technique to enhance the mixing rate of two miscible fluids with different viscosities in radial injection [30]. Ahmadlouydarab and colleagues investigated immiscible fluids displacement in the presence of phase change [31]. Their numerical results confirmed significant effects of the important parameters e.g., capillary and Jacob numbers and viscosity ratio on the interfacial development and fingering pattern. According to the results, increasing both capillary number and viscosity ratio and decreasing Jacob number amplified the interfacial instability [31]. Later, in 2016, Tiago, Lins, and Azaiez proposed a new technique called controlled injection where the flow was continually adjusted to reduce the interfacial instabilities, thereby controlling the fingering pattern [32]. After that, similar researches were conducted by the same research group on the time-dependent injection in radial fluid-fluid displacement [33, 34]. Surguchev examined the effects of the cyclic water injection on oil recovery from a heterogeneous reservoir and reported increased efficiency [35]. Li et al. investigated the control of finger development through adjustment of injection rates and determined that predicting and controlling finger patterns is extremely challenging. Their research emphasized that the flow rate controlling would results in interfacial stability [36]. Results for immiscible and slightly miscible fluids displacement, from Huang and Chen research, indicated that the linear injection method compared to the fixed injection method could significantly reduce finger instability and the length of the fluid-fluid interface. The length of the fluid-fluid interface is a common method for quantitative stability assessment, as longer contact length indicates more instability [37]. This parameter is particularly useful in reactive situations. Their study on intermittent injection revealed the formation of different fluid layers and increased contact surfaces between the fluids. Leshchiner et al., studied the growth of air bubbles in oil layers in a Hele-Shaw cell, resulting in an equation

for harmonic moments dynamics [38]. Elghawy et al. recently conducted a study on viscose fingering instability analysis inside a homogeneous porous media under time-dependent flow injection and suggested that by selecting appropriate parameters including period and amplitude the interfacial instability could be controlled [39].

Yuan et al. investigated the effects of simple periodic time-dependent displacement rates on viscous finger onset and development. Results indicated that increasing the period leads to more unstable displacement, and depending on periodicity, amplitude, and scenarios, it can either stabilize or destabilize the viscous finger [40].

Due to the complexity of the phenomenon and the large amount of data involved, numerical simulations are challenging and often fail to accurately describe finger structures. Research has shown how time-dependent injection can impact instability formation and growth. While the effect of injection rate has been studied in numerous researches, there is limited quantitative description of fingers

Overall, existing literature has mainly focused on experimental studies of fluid-fluid interfacial morphology under constant/transient injection or fluid suction alone. There is a lack of knowledge in exploring the effects of consecutive injection-suction on fluid-fluid interfacial development both theoretically and experimentally.

In current experimental study, in order to enhance the existing knowledge, we are interested in the following main goals during consecutive injection-suction of a Newtonian fluid at constant-flow rate, pseudo-sinusoidal, and percussive method at different flow rates to displace a Newtonian fluid:

1) Investigation of the consecutive injection-suction effects on interfacial behavior and morphology of two immiscible fluids.
2) Studying the effects of consecutive injection-suction repetition on the interfacial morphology and stability of fluid-fluid interface.
3) Investigation on the possibility of interfacial morphology reversibility from unstable condition to the initial stable condition after a cyclic repetition.
4)

2. EXPERIMENTAL SECTION

2.1. Experimental Setup

In this study, a transparent Hele-Shaw cell, a syringe pump, a camera, three different types of oil, water, and ink were employed. The equipment's operation is illustrated in Figure (2), and the experimental setup is depicted in Figure (3). The Hele-Shaw cell is comprised of one transparent and one opaque plates separated by a distance of 0.56 cm. The selected plates have a large thickness, and the dimensions of the Halle-Shaw tube are not selected too much until plates start to bend and come close to each other. On the other hand, the transparent plate is made of plexiglass and the white plate is made of Acrylonitrile butadiene styrene (ABS), both of which have very high physical and mechanical strength and are almost scratch-proof. Besides, both plates have very smooth surface. A tiny hole is drilled in the center of the top plate to insert the tip of the syringe. It worth mentioning that the Hele-Shaw is designed so that the plates can be easily opened and closed with bolts and nuts. Also, the leveler was used to control and measure the slope of the surfaces of the plates. Prior to commencing the injection process, the Hele-Shaw cell is filled with one of the oils listed in Table (1). The injectable fluid used is colored water with a droplet

of a blue ink added. Table (2) displays the surface tension data obtained for various fluids. Following each test, liquid soap or washing liquid was utilized to wash and clean the plates.

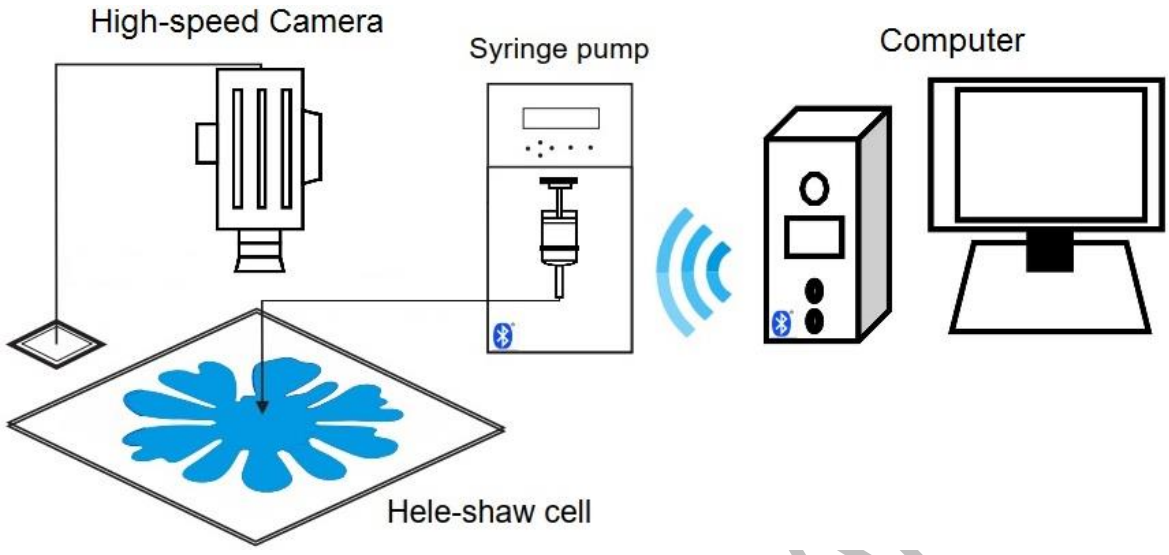

Figure 2: A schematic view from the experimental setup.

Table 1: Density and viscosity of the different oils.

Properties / Oil type	Measured viscosity at 25 °C (cP)	Measured viscosity at 40 °C (cP)	Measured viscosity at 100 °C (cP)	Measured density (kg/m^3)
1	151	71	10	895
2	920	421	50	869
3	1506	720	77	866

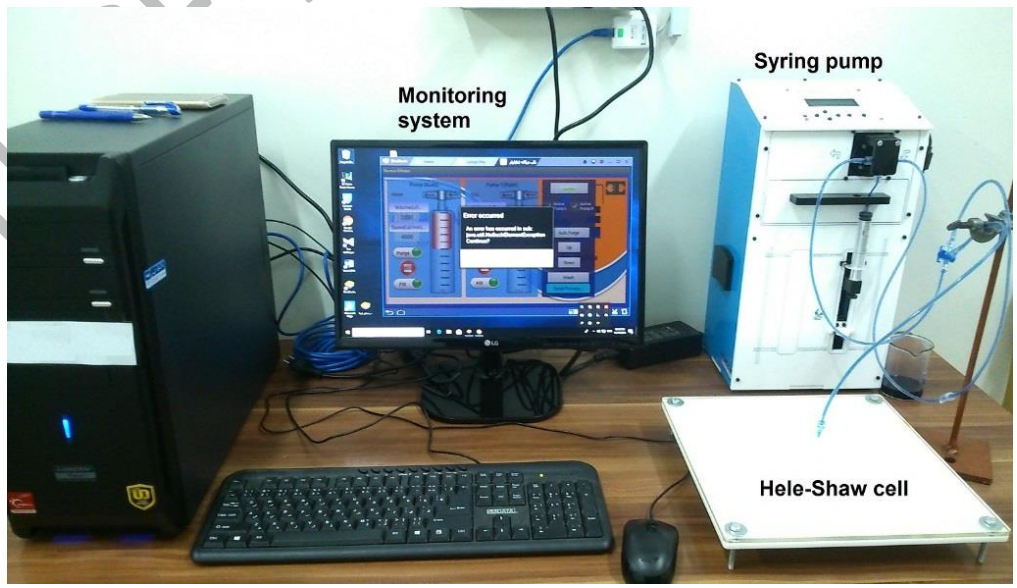

Figure 3: Experimental Hele-Shaw cell setup.

Table 2: Obtained surface tensions.

Setup fluids	Surface tension σ(mN/m)
Air and water	67
Air and Oil No. 1	31
Air and Oil No. 2	33
Air and Oil No. 3	35
Water and oil No. 1	36
Water and oil No. 2	33
Water and oil No. 3	32

2.2. Injection-suction methods

Three different forms of injection-suction methods including pseudo-sinusoidal, percussive, and constant flow rate were considered to reach the study goals. Table (3) shows details of the oils viscosity, and the flow rates for each method. Further explanation of the methods will be discussed in detail in the results section. All experiments took place in controlled in vitro conditions at 25°C and one atmosphere pressure. The area and perimeter of the fingers formed in the Hele-Shaw cell were measured by recording images from test videos and utilizing Digimizer software.

Table 3: Injection-suction of fluids using pseudo-sinusoidal, percussive, and constant flow rate methods

Injection-suction method	Oil viscosity (cP)	Flow Rate (m/min)
Pseudo-Sinusoidal	10	20
	50	10, 20, 30
	77	20
percussive	10	20
	50	10, 20, 30
	77	20
Constant-flow rate	50	2.666
	50	5.333
	50	8

2.3. Mathematical Equations

It is assumed that both displacing and displaced fluids are incompressible. For such a system, the momentum and continuity equations can be expressed in a dimensionless forms as Equations (1) and (2):

$$Re\left[\frac{\partial u^*}{\partial t^*} + \rho u^*.\nabla u^*\right] = \frac{Ca}{\alpha^2}(-\nabla p^* + \mu^*\nabla^2 u^*) \qquad (1)$$

$$\nabla u^* = 0 \quad (2)$$

The equation for the dimensionless injection flow rate can be written in a similar manner:

$$Q^*(t) = D \sin\left(\frac{2\pi t^*}{T^*}\right) \quad (3)$$

The dimensionless Capillary (*Ca*), Womersley (α), and Reynolds (*Re*) numbers can also be defined using specific equations:

$$Re = \frac{VH}{v} = \frac{\rho\, Q(t)\, H}{\mu A(t)} \quad (4)$$

$$Ca = \frac{R^2 Q(t)}{\sigma \beta A(t)} \quad (5)$$

$$\alpha^2 = \frac{2\pi H^2 \rho_2 \sigma Q(t)}{T \mu_2{}^2 u_{ave} A(t)} \quad (6)$$

Where, H, D, A(t), μ, Q(t), σ, ρ, R, and T are the distance between the two Hele-Shaw plates, instantaneous surface (The area is equal to the perimeter of the area occupied by injected fluid multiplied by gap size), viscosity, flow rate, surface tension, fluid density, instantaneous injection diameter, and period of each injection cycle, respectively. Besides, $Q^* = Q\sigma/(\mu_2 H \pi R_0^2)$, $\sigma^* = \beta_2 \sigma^2/(\mu_2 H R_0^3)$, $p^* = p\beta_2\sigma/(\mu_2 H R_0^2)$, $t^* = t\frac{\mu_2 H}{\sigma}$, $U^* = \frac{U\sigma}{\mu_2 H R_0}$, and $r^*=r/R_0$. Note that, the subscript (1) is for injected fluid, and subscript (2) is for oils. Also, R_0 is the initial radius of the spot where the injected water enters. Moreover, the radial position of the fluid-fluid interface is defined by $\mathcal{R}$ (θ, t). Where θ is the radial angle and t time. And finally, the mobility is defined as $\beta = \frac{H^2}{12\mu}$.

3. RESULTS AND DISCUSSION

3.1. Injection-suction using Pseudo-sinusoidal method

Figure 4 displays the full cycle of injection-suction with a maximum injection flow rate of 20 ml/min. The cycle lasts for a total of 180 seconds and is divided to 16 stages, with each stage containing 1 ml of fluid injection or suction. The cycle consists of 8 injection stages followed by 8 suction stages. The injection stages begin with stage 1, where fluid is injected at 2.5 ml/min for 24 seconds, followed by stages 2, 3, and 4 with increasing flow rates and decreasing injection times. The cycle then transitions to suction stages, with negative flow rates shown in Figure 4.

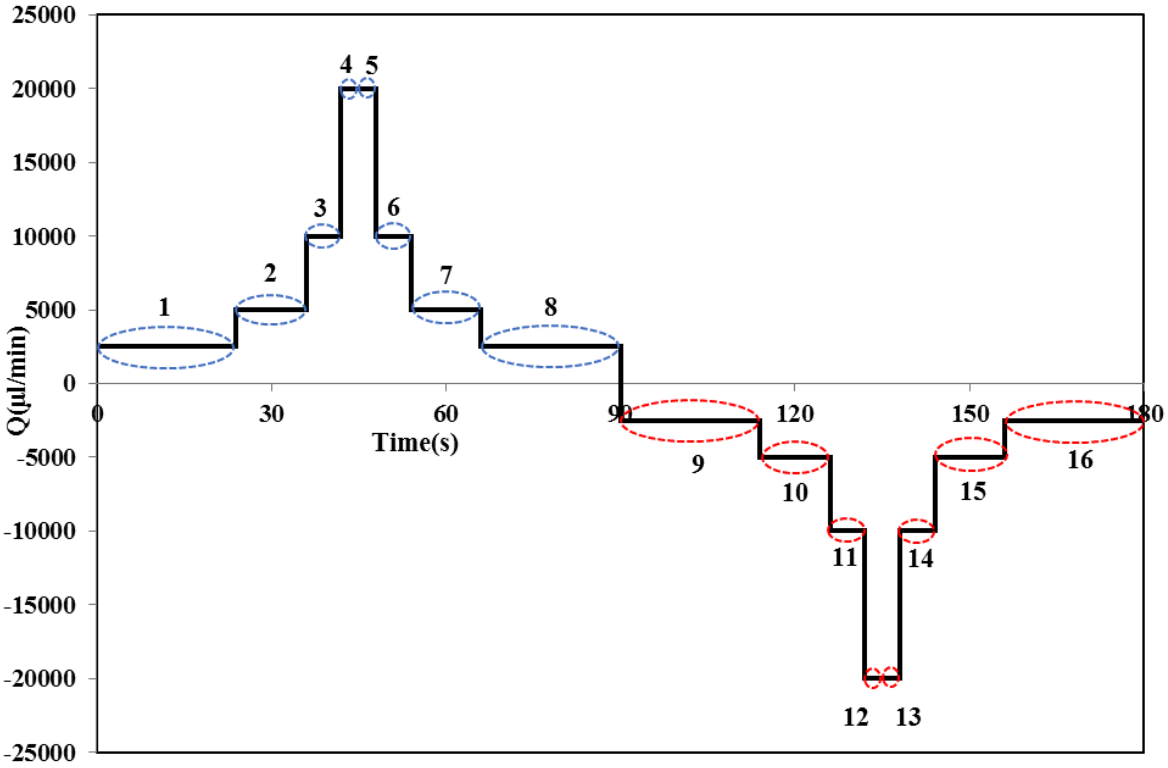

Figure 4. Total stages of the consecutive injection-suction in one Pseudo-sinusoidal cycle. The maximum injection-suction flow rate is 20 ml/min.

When using flow rates of 30 ml/min and 10 ml/min, the number of injection and suction stages remains consistent with those of the 20 ml/min flow rate, with each stage containing 1 ml of fluid. The difference lies in the duration of the stages and the overall cycle period, which varies based on the flow rate. The typical trend for all flow rates is shown in Figure 4. The period time of a full cycle at different flow rates has been displayed in Table 4. During experiments, five complete cycles are conducted and the results are compared together.

To study the changes in interfacial morphology at the fluid-fluid interface in the Pseudo-sinusoidal method, the results of the maximum flow rate of 20 ml/min are analyzed. Before the injection begins, a precise initial circle of the injected fluid with a radius of 1 cm is created in the center of the hele-shaw cell. Note that, the shape of this circle impacts how the fluid behaves in later stages.

Table 4. Periodic time of a cycle at different maximum flow rates in Pseudo-sinusoidal injection-suction method.

Flow rates (ml/min)	10	20	30
The periodic time of cycle (min)	6	3	2

In the first stage, when injection is initiated, the longest finger grows from 0.00 to 0.52 cm within 24 seconds. The growth rate of the finger length is slower in this stage due to the slower injection speed, resulting in a low capillary number.

Moving on to the second stage, the instability of the contact surfaces between the fluids increases with an increased flow rate, leading to the growth of finger numbers from 1 to 2. Over 12 seconds in this stage, the longest finger

grows from 0.52 cm to 1.24 cm, with a faster rate of growth compared to stage 1. In Figure 5, the morphology of the fluid-fluid interface at t=36s, end of the stage 2 and start of the stage 3, is illustrated.

In the third stage, within 6 seconds, the longest finger length grows from 1.24 cm to 1.88 cm and the total number of fingers reaches to 4. The changes in base radius is less than that of the longest finger, indicating a greater tendency for growth in finger length. As the flow arte of injection is increased so the capillary number is getting high.

In stage 4, the maximum injection flow rate occurs. This injection lasts for 3 seconds. During this injection, the longest finger length grows from 1.88 cm to ~2.53 cm. The number of the fingers grow more rapidly compared to the previous stages, increasing from 4 to 7. Because of the maximum flow rate, the higher capillary number is predicted. Meanwhile the moderate effective radius is observed.

Stage 5 is a repetition of stage 4, with equal injection times. As injection continues at the highest flow rate the, in stage 5, the number of fingers increases from 7 to 8. The growth rate of the longest finger is slower compared to the stage 4. Most fingers widen in this stage. Moreover, as injection continues at the highest flow rate the effective radius increases compared to the stage 4. The observed capillary numbers is the highest among the stages.

Moving to the stage 6, the flow rate falls in descending trend, and due to the reduction in the flow rate the fingers tend to expand more. As the injection still continues, the longest finger length increases from 2.82 cm to 3.55 cm in 6 seconds. The number of fingers increases from 8 to 10, and they become longer than those in the stage 5. The reduction in flow rate and increase in effective radius result in a decrease in capillary number, although it remains high and causes an increase in the number of fingers.

Stage 7 sees an increase in the length of the longest finger from 3.55 cm to 4.07 cm over 12 seconds. Despite the fingers becoming wider, there are no changes in the number of fingers, which remains at 10. The capillary number decreases due to a decrease in flow rate and increase in effective radius compared to the previous stage.

The injection phase of the first cycle finishes at the end of stage 8. The longest finger length reaches 4.45 cm within 24 seconds in stage 8. This stage also sees the maximum effective radius and minimum injection flow rate. Besides, the number of fingers remains constant in this stage.

The main distinction between the suction and injection phases lies in the movement of the displacing and displaced fluids. While water pushes oil outward during injection, oil pushes water inward during suction. The suction phase commences in stage 9 with the minimum flow rate, resulting in a decrease in the length of the longest finger while maintaining a constant number of fingers. All parameters in stage 9 mirror those of stage 8. The base radius increases, but the maximum finger radius decreases, leading to a reduction in the length of the largest finger from 4.52 cm to 4.18 cm in 24 seconds.

In the Stage 10, the trend of decreasing finger length continues, with the longest finger decreasing from 4.18 cm to 3.90 cm over 12 seconds. The injected fluid volume and flow rate match those of stage 7. As the fingers shrink, the base radius increases and the overall capillary number surpasses that of stage 9.

In stage 11, both base and the maximum finger radii decrease, a departure from the previous stages. Moreover, the longest finger decreases in length from 3.90 cm to 3.48 cm in 6 seconds.

The maximum suction flow rate is determined in stage 12, with the length of the longest finger decreasing from 3.48 cm to 2.95 cm in just 3 seconds. The change in the base radius length is minimal and can be considered constant.

Moving on to the stage 13, the base radius remains stable as in stage 12. Within another 3 seconds, the longest finger decreases in length from 2.95 cm to 2.23 cm. Both base and maximum finger radii also decrease during this stage.

When stage 14 starts, decrease in injection flow rate leads to a sharp reduction in the length of the longest finger from 2.23 to 1.32 cm within 6 seconds. The fingers become significantly smaller, with the number decreasing from 6 to 2.

As we enter stage 15, the length of the longest finger decreases from 1.32 to 0.32 cm, and the base radius undergoes a significant change. This reduction in the finger length intensifies due to a sharp decrease in water content inside the hele-shaw cell. Besides, the fingers are disappeared although the fluid-fluid interface dose not reach to a circular shape.

At the end of the stage 16, the base radius decreases and returns to the initial radius of the circle from stage 1 although it does not have a perfect circular shape. The main difference here is the irregularities in the circle's periphery caused by instabilities during the first injection-suction cycle from stages 1 to 16.

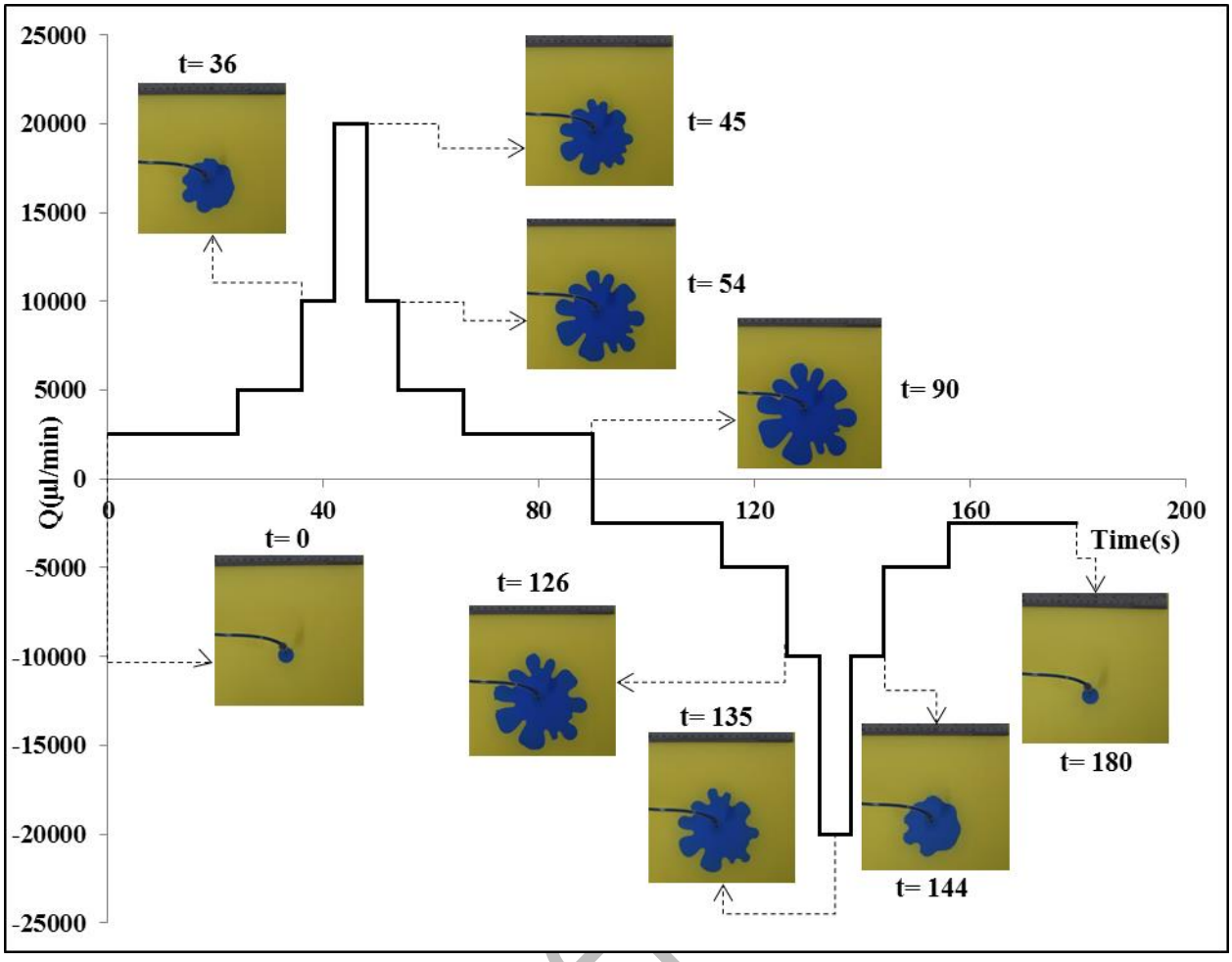

Figure 5. Fluid-fluid interfacial morphology development in the 1st cycle when the consecutive Pseudo-sinusoidal method is used at maximum injection/suction flow rate of 20 ml/min.

Figure (5) illustrates the interfacial morphology development in the first cycle when the consecutive Pseudo-sinusoidal method is used at maximum injection flow rate of 20 ml/min. Also, Table (5) provides details of the quantitative results of important parameters obtained from first cycle.

During the second cycle more instabilities are observed. In this cycle, the instabilities include the development of additional branches in the fingers, beginning at stage 6 and continuing through stage 13. Figure (6) displays the progression of the fluid-fluid interfacial morphology in the second cycle, revealing a higher level of instabilities compared to the first cycle.

When comparing the results from Figure (6) to those in Figure (5), a noticeable increase in instabilities can be observed in the second cycle when using consecutive pseudo-sinusoidal injection-suction method.

Table 5. Quantitative results of important parameters obtained from first cycle.

Stage	Time (s)	Fingers at beginning and end		Minimum and maximum longest finger	minimum and maximum r (cm)	minimum and maximum r_b (cm)
		Number	Branched			
1	0-24	0-1	0	0.00-0.52	1.08-3.00	1.08-2.48
2	24-36	1-2	0	0.52-1.24	3.00-4.13	2.48-2.90
3	36-42	2-4	0	1.24-1.88	4.13-4.85	2.90-2.97
4	42-45	4-7	0	1.88-2.53	4.85-5.62	2.97-3.09
5	45-48	7-8	0	2.53-2.82	5.62-5.96	3.09-3.14
6	48-54	8-10	0	2.82-3.55	5.96-6.78	3.14-3.23
7	54-66	10-10	0	3.55-4.07	6.78-7.34	3.23-3.27
8	66-90	10-10	0	4.07-4.52	7.34-7.88	3.27-3.37
9	90-114	10-10	0	4.52-4.18	7.88-7.59	3.37-3.41
10	114-126	10-10	0	4.18-3.90	7.59-7.33	3.41-3.48
11	126-132	10-9	0	3.90-3.48	7.33-6.92	3.48-3.44
12	132-135	9-8	0	3.48-2.95	6.92-6.39	3.44-3.44
13	135-138	8-6	0	2.95-2.23	6.39-5.60	3.44-3.33
14	138-144	6-2	0	2.23-1.32	5.60-4.60	3.33-3.28
15	144-156	2-0	0	1.32-0.32	4.60-3.18	3.28-2.86
16	156-180	0-0	0	0.32-0.00	3.18-1.19	2.86-1.19

To examine the impact of the cycles sequence on the development of interfacial morphology, the consecutive injection-suction process was repeated at least 5 times. The results suggest that more instabilities in the fifth cycle are likely to occur compared to the previous cycles. By stage 3 in the fifth cycle, the number of fingers reaches its maximum for that cycle. The length of the longest finger in stage 8 reaches 5.71 cm, signifying longer fingers compared to the earlier cycles. Additionally, in stages 9, 10, and 14, due to the higher effects of the suction on the end parts of the fingers the base radius starts to increase during suction stages. As the perfect circular shape of the initial injection circle cannot be reached at the end of the cycles, the remaining instabilities on the interface results in the increment of the he maximum number of branches which reaches 4.

Figure (7) illustrates the snapshots of the Fifth cycle's fluid-fluid interfacial morphology development using the pseudo-sinusoidal injection-suction method. Almost of the fingers in this cycle become wider and more symmetrical, with the base radius increasing in the stages 9 to 11 and also in stage 13 despite fluid suction.

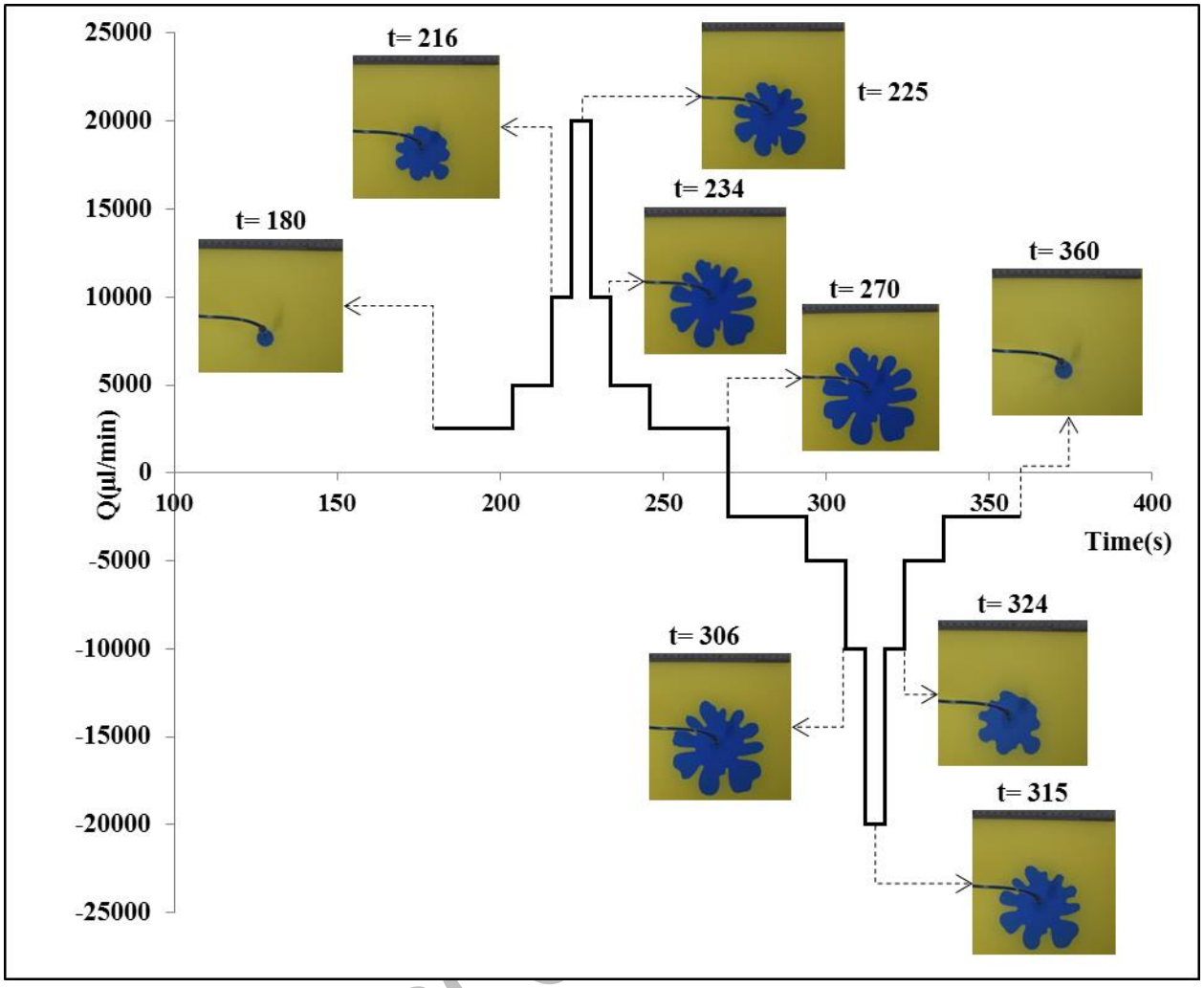

Figure 6. Snapshots of the fluid-fluid interfacial morphology development in the 2nd cycle when using the consecutive pseudo-sinusoidal method at maximum injection/suction flow rate of 20 ml/min.

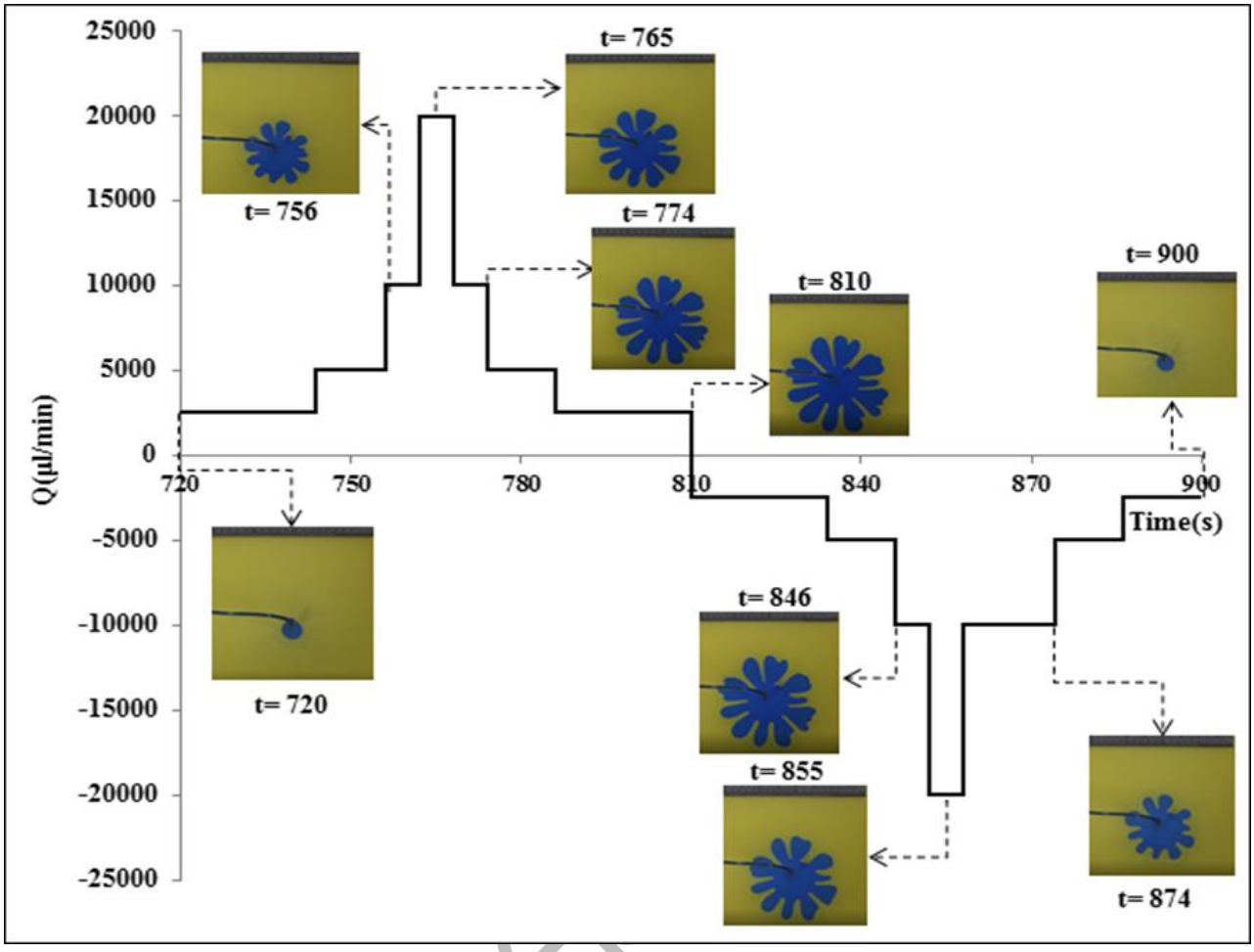

Figure 7. Snapshots of the fluid-fluid interfacial morphology development in the 5th cycle when using the consecutive pseudo-sinusoidal method at maximum injection/suction flow rate of 20 ml/min.

Table (6) shows the most important quantitative parameters measured/calculated in 1st, 2nd, and 5th cycles. Across all the stages, increasing the cycle number from 1 to 5, the quantity of the fingers increases so the length of the longest finger. In the 1st cycle, no branched fingers are observed, while in the second cycle, there are 3, and in the fifth cycle, there are 4 branched fingers. This illustrates that an increase in cycle number leads to a higher number of branched fingers. Moreover, appearance and disappearance of the branches occur at a faster rate.

Table 6. Quantitative parameters in the 1st, 2nd, and 5th cycles.

Stage	Time (s)	Number of fingers			Number of branched fingers			The length of the longest finger		
		1st cycle	2nd cycle	5th cycle	1st cycle	2nd cycle	5th cycle	1st cycle	2nd cycle	5th cycle
1	0-24	0-1	0-1	0-5	0	0-0	0-0	0.00-0.52	0-1.10	0.00-1.76
2	24-36	1-2	1-4	5-10	0	0-0	0-0	0.52-1.24	1.10-2.03	1.76-2.84
3	36-42	2-4	4-6	10-10	0	0-0	0-0	1.24-1.88	2.03-2.94	2.84-3.52
4	42-45	4-7	6-9	10-10	0	0-0	0-1	1.88-2.53	2.94-3.46	3.52-4.00
5	45-48	7-8	9-9	10-10	0	0-0	1-4	2.53-2.82	3.46-4.07	4.00-4.60
6	48-54	8-10	9-9	10-10	0	0-2	4-4	2.82-3.55	4.07-4.49	4.60-5.04
7	54-66	10-10	9-9	10-10	0	2-2	4-4	3.55-4.07	4.49-4.80	5.04-5.52
8	66-90	10-10	9-9	10-10	0	2-3	4-4	4.07-4.52	4.80-5.09	5.52-5.71
9	90-114	10-10	9-9	10-10	0	3-3	4-4	4.52-4.18	5.09-5.06	5.71-5.40
10	114-126	10-10	9-9	10-10	0	3-3	4-3	4.18-3.90	5.06-4.60	5.40-5.20
11	126-132	10-9	9-9	10-10	0	3-3	3-0	3.90-3.48	4.60-4.35	5.20-4.83
12	132-135	9-8	9-9	10-10	0	3-2	0-0	3.48-2.95	4.35-3.78	4.83-4.47
13	135-138	8-6	9-8	10-10	0	2-0	0-0	2.95-2.23	3.78-3.24	4.47-3.84
14	138-144	6-2	8-4	10-10	0	0-0	0-0	2.23-1.32	3.24-3.40	3.84-2.92
15	144-156	2-0	4-1	10-5	0	0-0	0-0	1.32-0.32	3.40-1.18	2.92-1.85
16	156-180	0-0	1-0	5-0	0	0-0	0-0	0.32-0.00	1.18-0.00	1.85-0.00

3.2. Consecutive percussive injection-suction method

This approach involves starting each cycle with the injection phase at its highest flow rate. The flow rate then decreases to its minimum level before rising back up to the maximum. Once the suction phase begins, the flow rate abruptly drops to its maximum suction level. Each stage involves injecting or suctioning 1 ml of fluid. The injection phase starts with a flow rate of 20 ml/min for 3 seconds in stage 1, followed by 10 ml/min for 6 seconds in stage 2, 5 ml/min for 12 seconds in stage 3, and 2.5 ml/min for 24 seconds in stage 4. The flow rate then increases in stages 5 to 8 before reaching 20 ml/min again in stage 8. The suction phase starts in stage 9, where the injected fluid is sucked out at flow rate of 20 ml/min. Figure (8) illustrates the 16 stages of the continuous percussive injection-suction method.

Figure 8. The total stages of the consecutive percussive injection-suction in a cycle at maximum injection/suction flow rate of 20 ml/min.

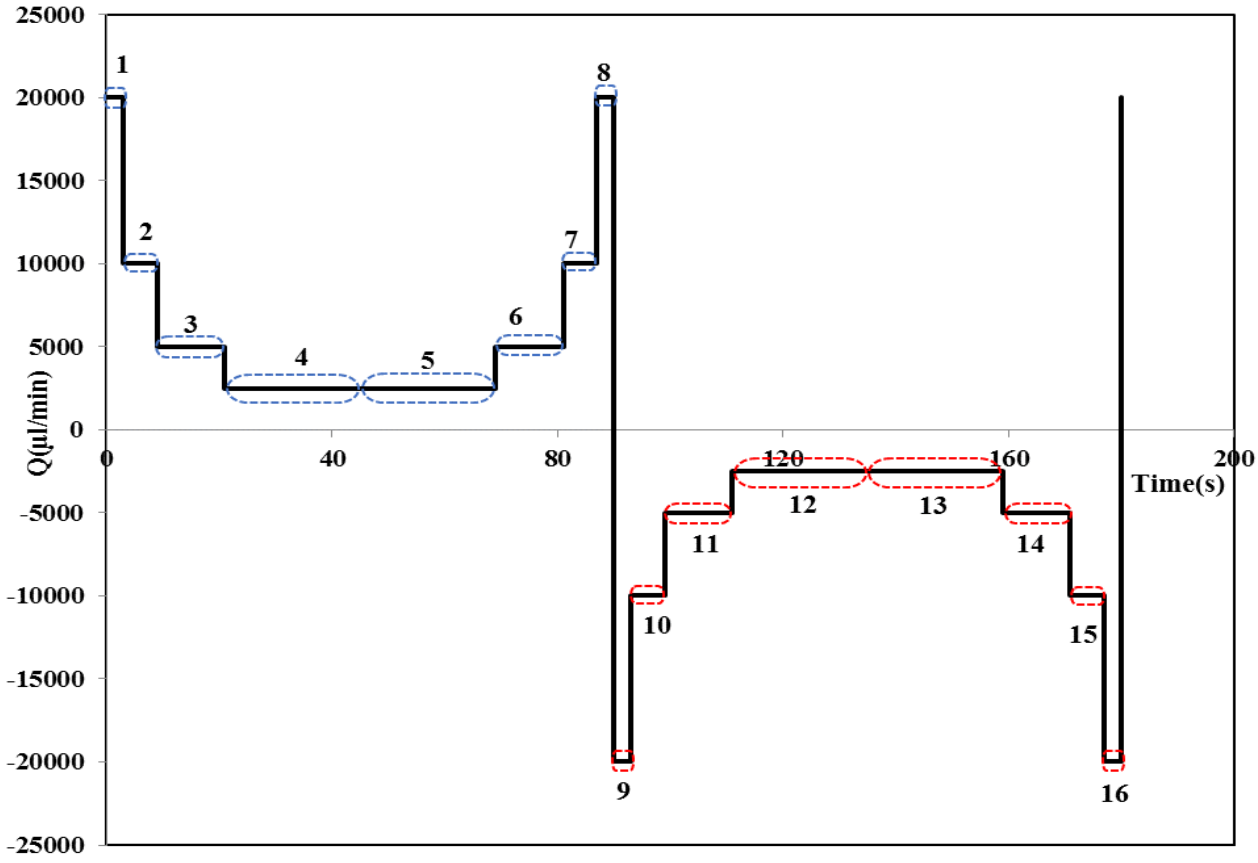

Table (7) displays calculated/measured important parameters in each stage of the 1st cycle. As it is shown in the table, longest finger in the 1st cycle of the percussive injection-suction method measures 5.36 cm. The length of fingers in this method exceeds that of the first cycle in the pseudo-sinusoidal injection-suction method. The maximum number of fingers seen is 12, with 2 fingers exhibiting branching. There is not any pockets or droplets during the injection-suction process in this cycle. Figure (9) provides few photos of the fluid-fluid interface development throughout the 16 stages in the 1st cycle. Once the injection phase begins at the highest flow rate, numerous fingers are observed within 9 seconds. Note that, the fingers become longer and wider y end of the stage 8th.

Table 7. Quantitative results of important parameters obtained from 1st cycle in injection-suction process using the percussive method.

Stage	Time (s)	Fingers		Longest finger length (cm)	minimum and maximum r (cm)	minimum and maximum r_b (cm)
		Number	Branched			
1	0-3	0-6	0-0	0.00-1.69	0.93-3.32	0.93-1.62
2	3-9	6-11	0-2	1.69-2.70	3.32-4.35	1.62-1.66
3	9-21	11-11	2-2	2.70-3.40	4.35-5.20	1.66-1.80
4	21-45	11-12	2-2	3.40-3.92	5.20-5.87	1.80-1.95
5	45-69	12-12	2-1	3.92-4.38	5.87-6.37	1.95-1.99
6	69-81	12-12	1-1	4.38-4.68	6.37-6.70	1.99-2.01
7	81-87	12-12	1-1	4.68-5.06	6.70-7.12	2.01-2.06
8	87-90	12-12	1-1	5.06-5.36	7.12-7.45	2.06-2.08
9	90-93	12-12	1-1	5.36-5.26	7.45-7.34	2.08-2.07
10	93-99	12-12	1-1	5.26-4.84	7.34-6.97	2.07-2.13
11	99-111	12-12	1-1	4.84-4.553	6.97-6.67	2.13-2.12
12	111-135	12-11	1-1	4.55-4.13	6.67-6.32	2.12-2.19
13	135-159	11-11	1-0	4.13-3.67	6.32-5.80	2.19-2.13
14	159-171	11-9	0-0	3.67-2.96	5.80-5.08	2.13-2.12
15	171-177	9-3	0-0	2.96-2.03	5.08-4.10	2.12-2.08
16	177-180	3-0	0-0	2.03-0.00	4.10-1.11	2.08-1.11

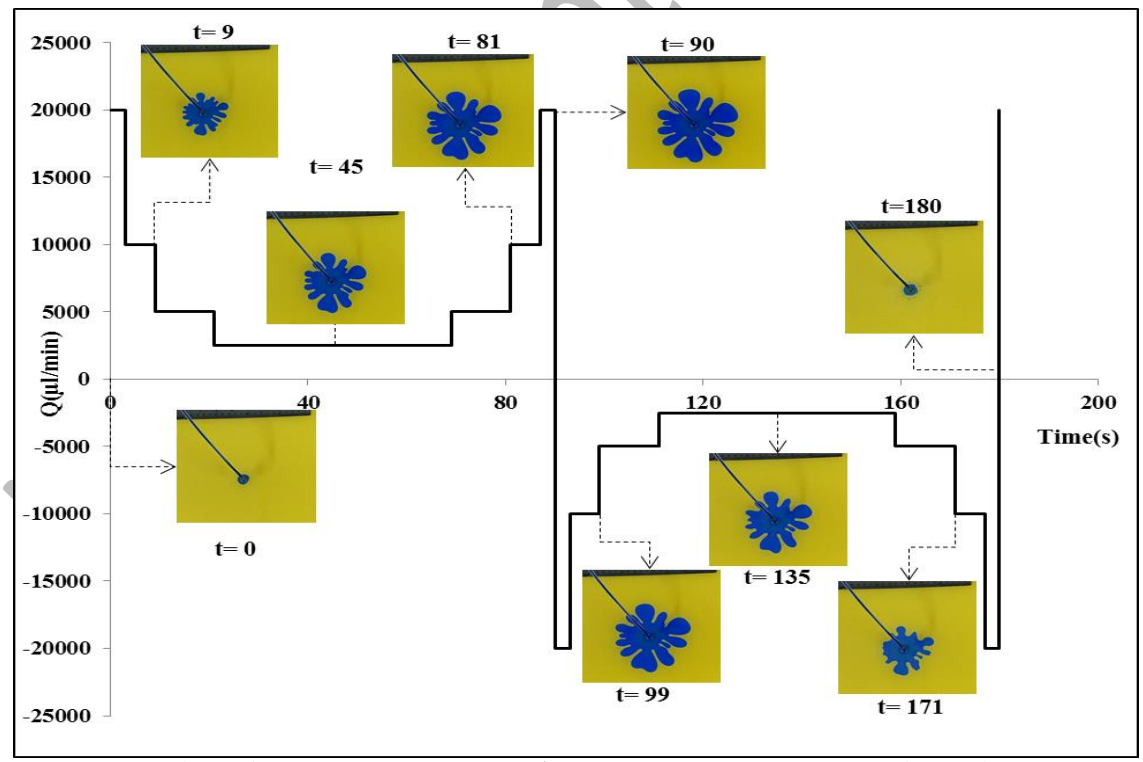

Figure 9. Snapshot of the interfacial morphology development in the 1st cycle when the percussive method at maximum flow rate of 20 ml/min is used.

Beginning of the stage 9 is start for suction phase. This phase starts at maximum flow rate of 20 ml/min, causing the fingertips to be pulled inwards due to increased capillary forces directed towards the injection center. The

snapshots in Figure 9 clearly show this inward stretching during the injection phase, resulting in a reduction in finger length.

Overall, results indicate that, in the second cycle, there is an increase in the number of fingers, droplets, oil pockets, finger branches, and fingers length in comparison with the 1st cycle. From stages 11 to 15, despite fluid suction from the center, the base radius increases because of the fingers' length reduction and fluid moving towards the center of the cell. Initially, the suction affects the fingers' length. Table (8) displays various parameters for each stage during the 2nd cycle.

Table 8. Calculated/measured important quantities in second cycle when the percussive method at maximum injection flow rate of 20 ml/min is used.

Stage	Start and end time of stages	Fingers		Number of droplets	Number of pockets	longest finger range (cm)	minimum and maximum r (cm)	minimum and maximum r_b (cm)
		Number	Branched					
1	0-3	0-21	0-0	0-4	0-1	0.00-2.29	1.11-3.81	1.11-1.52
2	3-9	21-21	0-0	4-8	1-1	2.29-3.24	3.81-4.94	1.52-1.70
3	9-21	21-21	0-1	8-9	1-1	3.24-3.83	4.94-5.61	1.70-1.78
4	21-45	21-18	1-2	9-10	1-1	3.83-4.36	5.61-6.31	1.78-1.96
5	45-69	18-17	2-3	10-10	1-1	4.36-4.80	6.31-6.80	1.96-2.00
6	69-81	17-17	3-3	10-10	1-1	4.80-5.18	6.80-7.26	2.00-2.09
7	81-87	17-17	3-3	10-8	1-1	5.18-5.51	7.26-7.64	2.09-2.13
8	87-90	17-17	3-3	8-8	1-1	5.51-5.82	7.64-7.97	2.13-2.15
9	90-93	17-17	3-3	8-8	1-1	5.82-5.68	7.97-7.80	2.15-2.12
10	93-99	17-17	3-3	8-9	1-1	5.68-5.39	7.80-7.43	2.12-2.04
11	99-111	17-17	3-3	9-9	1-1	5.39-4.99	7.43-7.11	2.04-2.12
12	111-135	17-16	3-3	9-10	1-1	4.99-4.61	7.11-6.74	2.12-2.13
13	135-159	16-16	3-2	10-8	1-1	4.61-4.18	6.74-6.32	2.13-2.14
14	159-171	16-16	2-2	8-8	1-1	4.18-3.50	6.32-5.59	2.14-2.09
15	171-177	16-16	2-1	8-8	1-1	3.50-2.45	5.59-4.61	2.09-2.17
16	177-180	16-0	1-0	8-2	1-0	2.45-0.47	4.61-1.48	2.17-1.01

Figure (10) shows few photos from fluid-fluid interfacial development during the 2nd cycle. Similar to the 1st cycle, fluid injection starts with the highest flow rate. However, compared to the 1st cycle, the fingers have narrower shape and also they are longer. Few oil pockets are present inside the injected fluid in the 1st stage of the 2nd cycle, continuing until the end of the cycle.

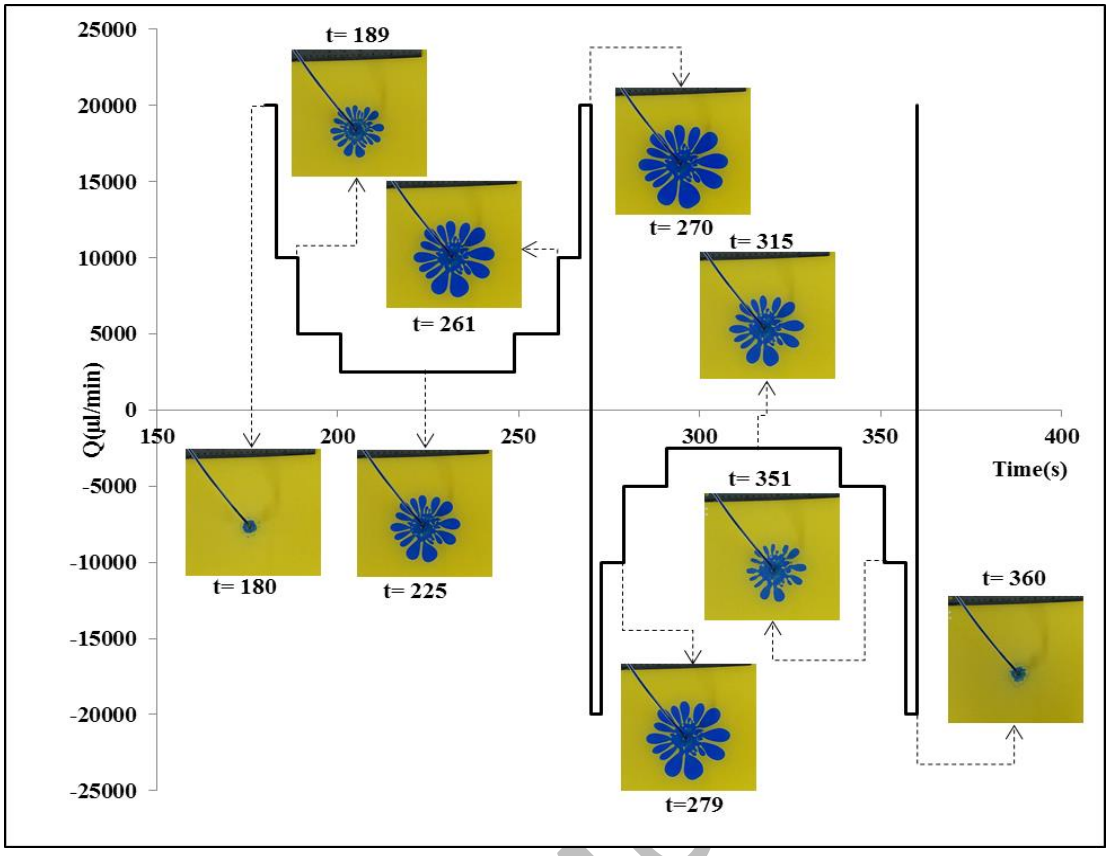

Figure 10. Interfacial morphologies of the fluid-fluid interface in the 2nd cycle when the percussive method is used at maximum flow rate of 20 ml/min.

Table 9. Calculated/measured quantities in the 5th cycle when percussive method is used.

Stage	Time (s)	Fingers		Number of droplets	Number of pockets	longest finger range (cm)	minimum and maximum r (cm)	minimum and maximum rb (cm)
		Number	Branched					
1	0-3	0-17	0-5	4-5	6-21	1.25-2.76	1.97-4.56	0.72-1.80
2	3-9	17-17	5-5	5-4	21-34	2.76-3.68	4.56-5.65	1.80-1.97
3	9-21	17-16	5-5	4-3	34-38	3.68-4.30	5.65-6.38	1.97-2.08
4	21-45	16-14	5-4	3-3	38-38	4.30-4.75	6.38-6.97	2.08-2.23
5	45-69	14-14	4-3	3-3	38-38	4.75-5.26	6.97-7.59	2.23-2.33
6	69-81	14-14	3-3	3-3	38-38	5.26-5.59	7.59-7.93	2.33-2.35
7	81-87	14-14	3-3	3-3	38-38	5.59-5.95	7.93-8.31	2.35-2.36
8	87-90	14-14	3-4	3-3	38-38	5.95-6.18	8.31-8.58	2.36-2.40
9	90-93	14-14	4-4	3-3	38-38	6.18-6.09	8.58-8.47	2.40-2.38
10	93-99	14-14	4-3	3-3	38-38	6.09-5.84	8.47-8.24	2.38-2.41
11	99-111	14-14	3-3	3-3	38-38	5.84-5.58	8.24-7.94	2.41-2.36
12	111-135	14-14	3-3	3-3	38-38	5.58-5.03	7.94-7.43	2.36-2.40
13	135-159	14-14	3-3	3-3	38-38	5.03-4.25	7.43-6.83	2.40-2.49
14	159-171	14-13	3-3	3-3	38-38	4.25-3.83	6.83-6.27	2.49-2.44
15	171-177	13-8	3-1	3-4	38-38	3.83-3.10	6.27-5.48	2.44-2.39
16	177-180	8-0	1-0	4-6	38-5	3.10-1.40	5.48-2.15	2.39-0.76

As shown in Table 9, the maximum number of the droplets and fingers falls to 17 and 5, respectively, which are lower than those of the 2nd cycle meanwhile the number of the oil pockets increases from 1 in the 2nd cycle to 38 in the 5th cycle. In most suction stages, similar to the 2nd cycle, the base radius increases. Figure (11) displays

snapshots of fluid-fluid interfacial development in the 5th cycle, showing fingers with fat fingertips and numerous oil pockets and droplets of displacing fluid.

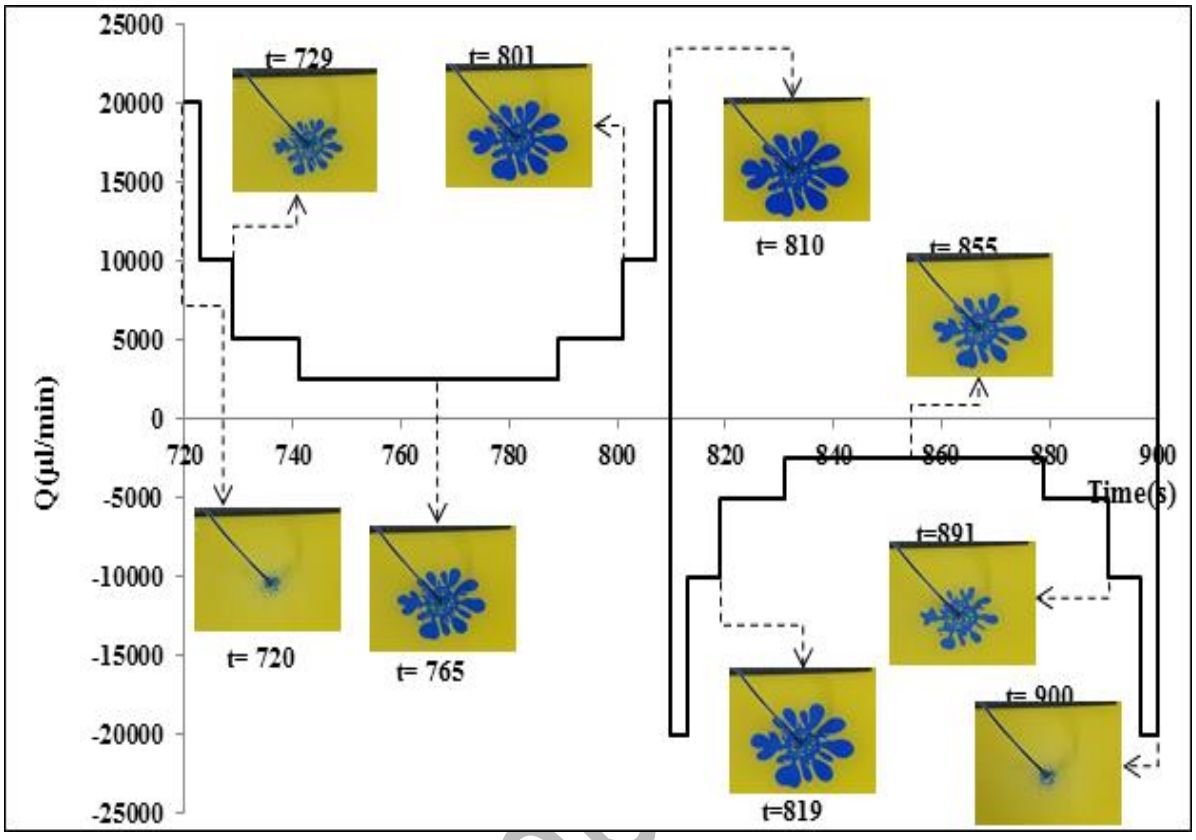

Figure 11. Interfacial morphologies of the fluid-fluid interface in different stages in the 5th cycle when the maximum flow rate is 20 ml/min.

Comparing the results of the 1st, 2nd, and 5th cycle together does not reveal a clear pattern in the number of fingers. However, examining the interfacial development results indicates a direct correlation between the number of fingers and their narrowness or width. In the 2nd cycle, however, the narrower fingers result in a higher number of fingers compared to the 1st and 5th cycles. Despite this, generally, the fingers length tends to increase with increasing the cycle number. For instance, the longest finger in cycle 1 measures 5.36 cm, while in the 2nd and 5th cycles it measures 5.81 cm and 6.18 cm, respectively.

In addition to the increase in finger length, each cycle also sees a rise in the branched fingers quantity. Furthermore, the time taken for fingers to branch is shorter than the time for the branching to disappear during the injection phase compared to the suction phase.

Overall, oil pockets quantity, in the percussive method, is strongly influenced by the number of cycles. This is evident as the pockets go from being absent in the 1st cycle to 38 in the 5th cycle. Additionally, droplets start to form from the 2nd cycle of this method. This is attributed to a sharp reduction in the injection/suction flow rate within the cycle. This rapid change does not allow sufficient time for a gradual alteration in the fingers' morphology, leading to the formation of droplets as parts of the fingers are cut off during the contraction process.

3.3. Consecutive constant-flow rate

In this method, there is a consistent fluid flow rate during both injection and suction stages. The amount of the fluid injected or sucked and the cycle period remain the same as in the other methods.

In the constant-flow rate method, a flow rate of 5.333 ml/min is maintained to ensure consistency with other injection-suction methods as the average injection-suction flow rate for others is 5.333 ml/min.

During each cycle in the constant-flow rate method, both the injection and suction phases involve 8 ml of fluid being transferred over 90 seconds at the selected flow rate of 5.333 ml/min.

To simplify the process, the whole phases are further divided into 15-second intervals, resulting in the cycle being divided into 12 stages - 6 for injection and 6 for suction, as illustrated in Figure 12.

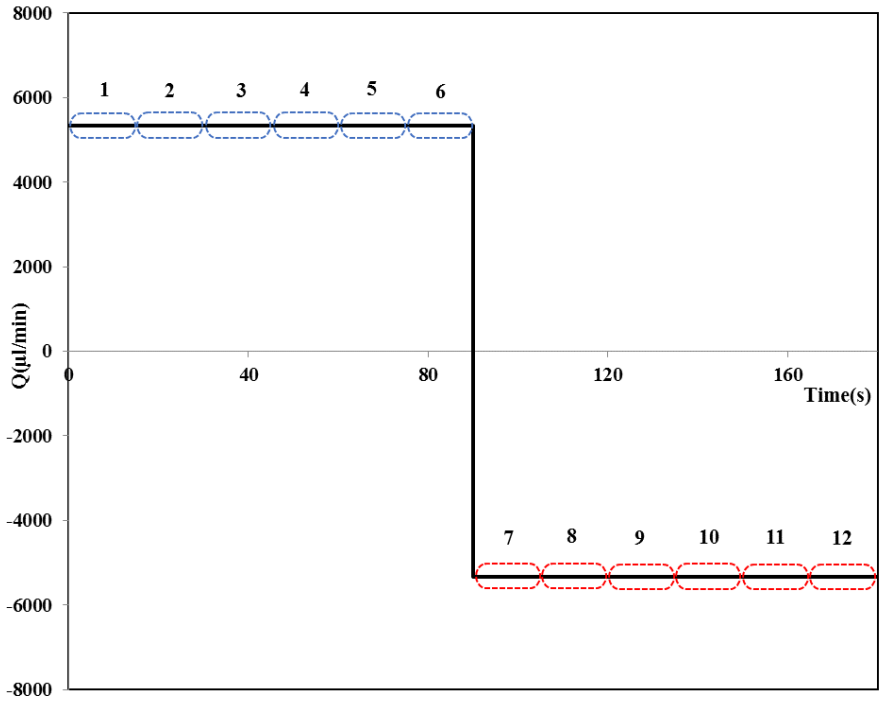

Figure 12. Total stages of the consecutive constant-flow rate injection-suction in one cycle. The maximum flow rate is 5.333 ml/min.

Table 10. Calculated/measured quantities in the 1st cycle when constant-flow rate method at flow rate of 5.333 ml/min was used.

stage	Time (s)	Fingers		longest finger range (cm)	minimum and maximum r (cm)	minimum and maximum r_b (cm)
		Number	Branched			
1	0-15	0-1	0	0.00-0.67	1.02-3.21	1.02-2.54
2	15-30	1-3	0	0.67-1.25	3.21-4.62	2.54-3.37
3	30-45	3-5	0	1.25-2.03	4.62-5.60	3.37-3.57
4	45-60	5-6	0	2.03-2.61	5.60-6.27	3.57-3.66
5	60-75	6-7	0	2.61-3.06	6.27-6.89	3.66-3.83
6	75-90	7-9	0	3.06-3.46	6.89-7.38	3.83-3.92
7	90-105	9-7	0	3.46-3.18	7.38-7.13	3.92-3.96
8	105-120	7-7	0	3.18-2.83	7.13-6.78	3.96-3.95
9	120-135	7-6	0	2.83-2.46	6.78-6.26	3.95-3.80
10	135-150	6-4	0	2.46-1.75	6.26-5.29	3.80-3.54
11	150-165	4-1	0	1.75-0.71	5.29-3.68	3.54-2.97
12	165-180	1-0	0	0.71-0.29	3.68-1.30	2.97-1.01

Table 10 displays the quantitative outcomes of the initial injection-suction cycle. During this cycle, the longest finger elongates to 7.38 cm. Notably, there are no observed droplets, pockets, or bifurcations, and the number of fingers peaks at 9. Surprisingly, in stage 7, both the base radius length and the longest finger length experience an increase, even though this stage falls within the suction phase.This anomaly can be attributed to the inertia of the injected fluid persisting from the prior 6 injection stages representations of the evolution of the two fluid interface throughout the injection-suction stages within the initial cycle, utilizing a constant-flow rate method with an injection, causing a radial outward push on the fluid-fluid interface. Figure 13 provides visual flow rate of 5.333 ml/min.

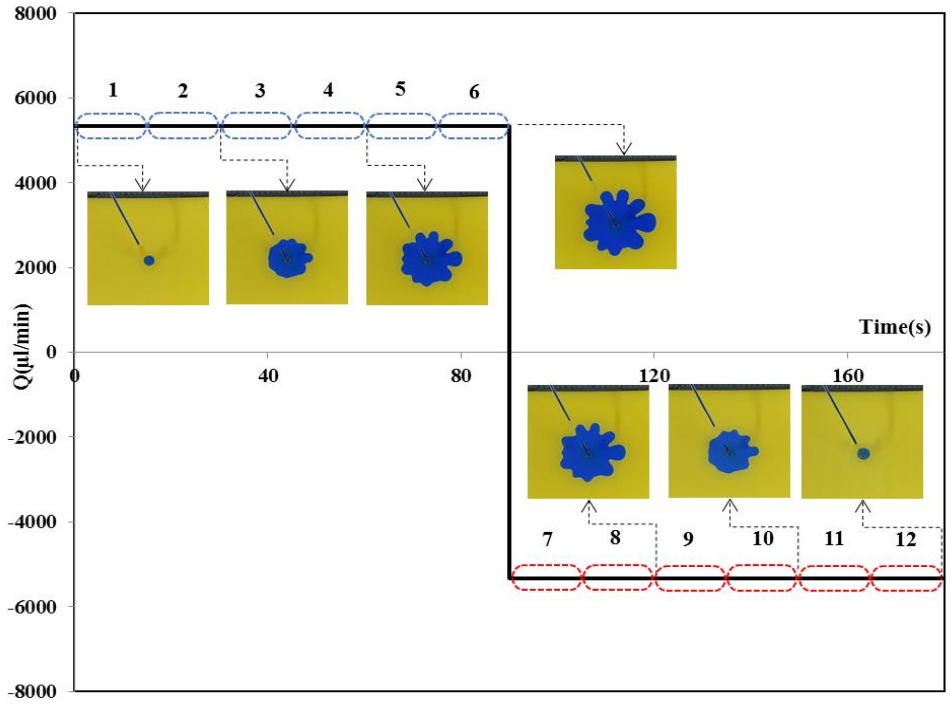

Figure 13. Snapshots of the interfacial morphology development in the 1st cycle when the constant-flow rate method with maximum flow rate of 5.333 ml/min was used.

In the 2nd cycle, similar outcomes were achieved, with no oil droplets or pockets identified. Table 11 reveals that the longest finger's length by the end of stage six measures 6.49 cm. The count of droplets, pockets, and branches within the fingers stands at 5, 8, and 2, respectively. Furthermore, the total number of fingers increases to 14. During stage 7, the initial phase of suction, the base radius achieves its peak value of 2.180 cm. However, starting from stage 8 until the conclusion of the suction phase, the base radius diminishes. Figure 14 illustrates snapshots illustrating the progression of the fluid-fluid interface throughout the 5th cycle. Notably, the presence of oil pockets is clearly visible in this depiction.

Table 11. Calculated/measured quantities in the 5th cycle when constant-flow rate method at flow rate of 5.333 ml/min was used.

stage	Start and end time of stages	Fingers		Number of droplets	Number of pockets	longest finger range (cm)	minimum and maximum r (cm)	minimum and maximum r_b (cm)
		Number	Branched					
1	0-15	0-13	0-1	4-5	0-8	0.53-3.06	1.76-4.87	1.23-1.81
2	15-30	13-13	1-1	5-4	8-8	3.06-4.46	4.87-6.32	1.81-1.86
3	30-45	13-13	1-1	4-3	8-8	4.46-5.14	6.32-7.21	1.86-2.07
4	45-60	13-13	1-2	3-3	8-8	5.14-5.76	7.21-7.85	2.07-2.09
5	60-75	13-13	2-2	3-3	8-8	5.76-6.30	7.85-8.38	2.09-2.09
6	75-90	13-13	2-2	3-3	8-8	6.30-6.64	8.38-8.80	2.09-2.16
7	90-105	13-13	2-2	3-3	8-8	6.64-6.49	8.80-8.67	2.16-2.18
8	105-120	13-13	2-2	3-3	8-8	6.49-6.29	8.67-8.43	2.18-2.14
9	120-135	13-13	2-2	3-3	8-8	6.29-5.75	8.43-7.90	2.14-2.15
10	135-150	13-13	2-1	3-3	8-8	5.75-4.971	7.90-7.11	2.15-2.14
11	150-165	13-13	1-1	3-3	8-8	4.97-3.71	7.11-5.90	2.14-2.20
12	165-180	13-0	1-0	3-3	8-0	3.71-0.53	5.90-1.78	2.20-1.25

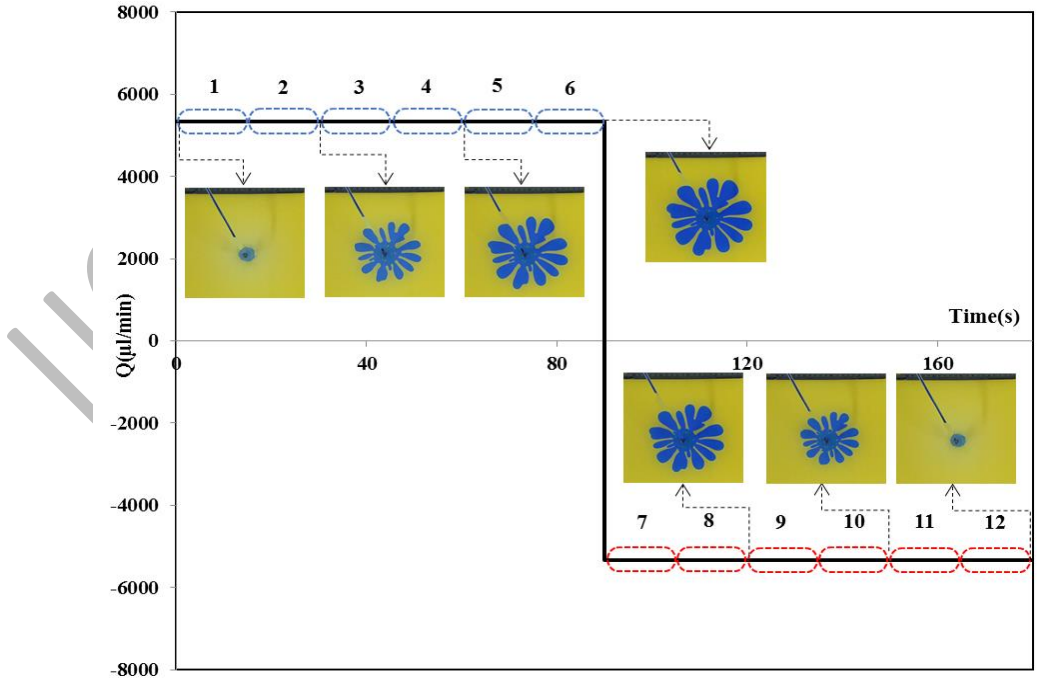

Figure 14. Snapshots of the interfacial morphology development in different stages in the 5th cycle when the constant-flow rate method at maximum flow rate of 5.333 ml/min was used.

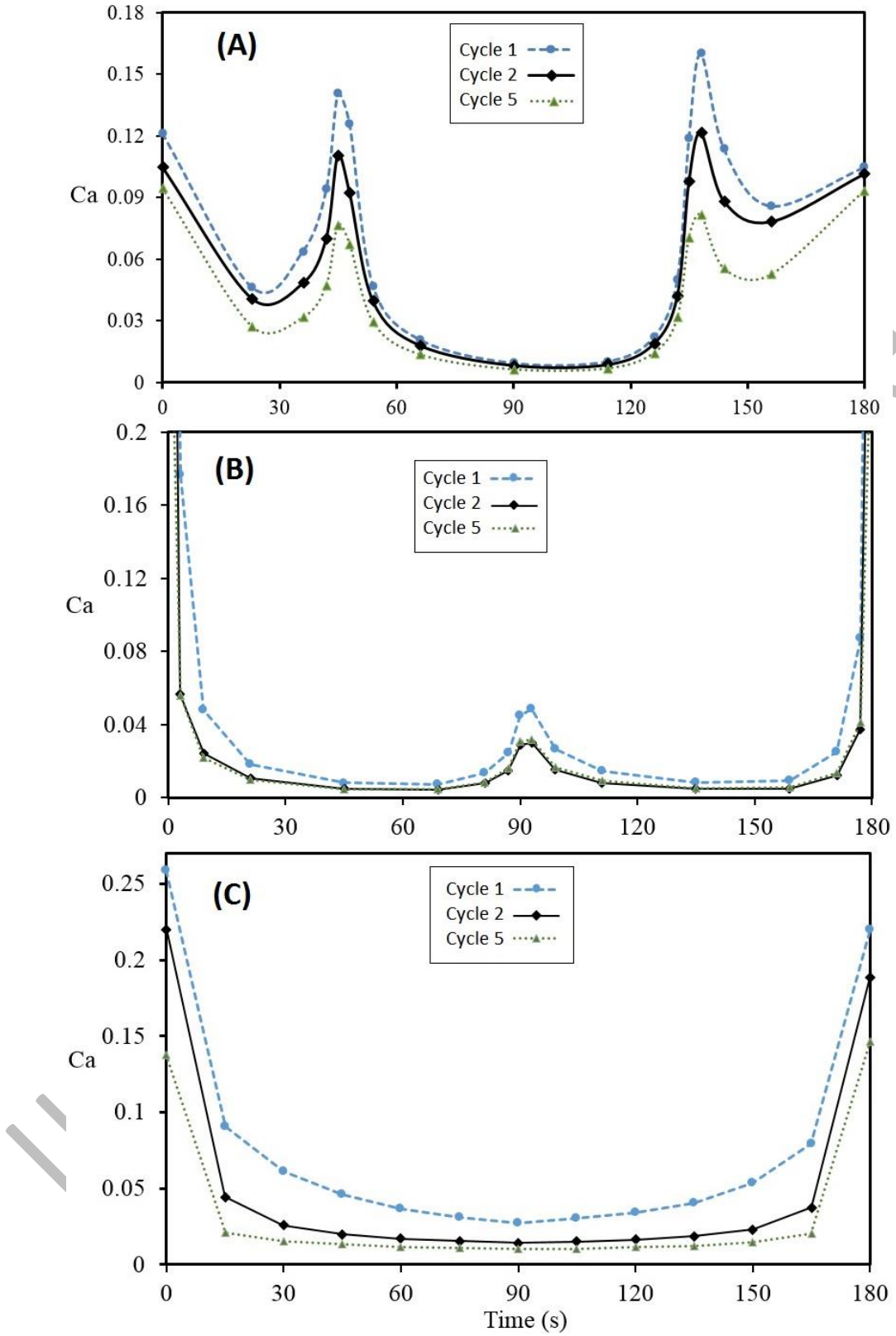

Figure 15. Variation of capillary number during 1st, 2nd, and 5th cycles for three different consecutive methods; (A) pseudo-sinusoidal, (B) percussive, and (C) constant-flow rate injection-suction. The maximum flow rate is 20 ml/min.

Figure 15 depicts the fluctuation of the capillary number across the 1st, 2nd, and 5th cycles for consecutive pseudo-sinusoidal, percussive, and constant flow-rate injection-suction techniques at a maximum flow rate of 20

ml/min. The graph illustrates significant shifts in capillary numbers when the injection or suction flow rates experience abrupt changes, particularly at the onset or conclusion of the cycles. Additionally, for all three methods, there is an observed trend of decreasing calculated capillary numbers with an increase in cycle number.

The decrease in the Ca value is particularly noticeable when the capillary number is high (Ca > ~0.05) in a cycle, indicating the influence of inertial forces. It is important to acknowledge that over subsequent cycles, the discrepancies among the curves should diminish, barring factors such as interfacial instabilities and computational inaccuracies.

4. CONCLUSIONS

This experimental study focused on analyzing the interfacial morphology dynamics of two immiscible Newtonian fluids within a Hele-Shaw cell during consecutive injection-suction cycles. The utilized fluids were water and base oil. Three different base oils with viscosities of 150, 920, and 1506 cP were used in the injection-suction cycles at maximum flow rates of 10, 20, and 30 ml/min for pseudo-sinusoidal, percussive time-dependent, and constant flow-rate methods. The injection and suction volumes were kept constant across all methods, and each method was repeated for a minimum of five complete cycles.

The primary aim was to investigate the suppression of interfacial instabilities and restore the initial perfect circular interface shape at the end of each cycle. Notably, the results concluded that restoring the initial morphology was challenging for percussive and constant flow-rate methods due to inertia effects. The growth rate of interfacial instabilities was slower in the pseudo-sinusoidal method compared to the other two methods. Similar to the constant flow injection, the lower viscosity or flow rate in the injection-suction process led to more stability.

The outcome of the study highlighted that an increase in flow rate results in a high number of the oil packets in the constant flow-rate method and the opposite in the reverse percussive injection-suction method. The pseudo-sinusoidal method did not exhibit instabilities like oil packets, water droplets, or fingers, which were prominent in the constant and percussive injection-suction methods.

Analysis of the capillary numbers across different injection-suction methods revealed abrupt changes in capillary number values with sharp alterations in flow rates at the beginning or end of cycles. Moreover, increasing the cycle number decreased the calculated capillary number, particularly for high values, although discrepancies between curves were expected to decrease with more cycles, barring interfacial instabilities and calculation errors.

In conclusion, based on the experiment conditions, the pseudo-sinusoidal method was identified as the most effective technique for restoring the stable fluid-fluid interface. However, increasing the number of cycles may amplify instabilities, making it challenging to maintain the initial stable interface condition.

REFERENCES

[1] Hill, S.; Inst, F., Channeling in packed columns. *Chemical Engineering Science*, 1 (6): 247-253 (1952).

[2] Slobod, R. L.; Caudle, B. H., X-Ray Shadowgraph Studies of Areal Sweep out Efficiencies. *Society of Petroleum Engineers*, SPE-211-G (1952).

[3] Saffman, P. G.; Taylor, G. I., The penetration of a fluid into a porous medium or Hele-Shaw cell containing a more viscous liquid. *Proceedings of the Royal Society A. Mathematical Physical and Engineering Sciences*, 245 (1242): 312-329 (1958).

[4] Chen, J. D., Radial viscous fingering patterns in Hele-Shaw cells. *Experiments in Fluids*, 5: 363–371 (1987).

[5] Park, C. W.; Homsy, G. M., The instability of long fingers in Hele–Shaw flows. *The Physics of Fluids*, 28: 1583 (1985).

[6] Nittmann, J.; Daccord, G.; Stanley, H. E., Fractal growth viscous fingers: quantitative characterization of a fluid instability phenomenon. *Nature*, 314: 141–144 (1985).

[7] Singh, B. K.; Azaiez, J., Numerical simulation of viscous fingering of shear-thinning fluids. *The Canadian Journal of Chemical Engineering*, 79 (6): 961-967 (2001).

[8] Ben-Jacob, E.; Garik, P., The formation of patterns in non-equilibrium growth. *Nature*, 343: 523–530 (1990).

[9] Yortsos, Y. C.; Zeybek, M., Dispersion driven instability in miscible displacement in porous media. *The Physics of Fluids*, 31: 3511 (1988).

[10] Zimmerman, W. B.; Homsy, G. M., Viscous fingering in miscible displacements: Unification of effects of viscosity contrast, anisotropic dispersion, and velocity dependence of dispersion on nonlinear finger propagation. *Physics of Fluids A: Fluid Dynamics*, 4: 2348 (1992).

[11] Zhao, H.; Casademunt, J.; Yeung, C.; Maher, J. V., Perturbing Hele-Shaw flow with a small gap gradient. *Phys. Rev. A*, 45: 2455 (1992).

[12] Manickam, O.; Homsy, G. M., Fingering instabilities in vertical miscible displacement flows in porous media. *Journal of Fluid Mechanics*, 288: 75-102 (1995).

[13] Ruith, M.; Meiburg, E., Miscible rectilinear displacements with gravity override. *Journal of Fluid Mechanics*, 420: 225-257 (2000).

[14] Homsy, G. M., Viscous fingering in porous media. *Annual review of fluid mechanics*, 19: 271-311 (1987).

[15] Yortsos, Y. C., The relationship between immiscible and miscible displacement in porous media. *AIChE journal*, 33 (11): 1912-1915 (1987).

[16] McCloud, K. V.; Maher, J. V., Experimental perturbations to Saffman-Taylor flow. *Physics Reports*, 260 (3): 139-185 (1995).

[17] Bataille, J., Stabilité d'un écoulement radial non miscible. *Revue Inst. Pétrole*, 23: 1349-1364 (1968).

[18] Paterson, L., Radial fingering in a Hele Shaw cell. *Journal of Fluid Mechanics*, 113: 513-529 (1981).

[19] Cardoso, S. S.; Woods, A. W., The formation of drops through viscous instability. *Journal of Fluid Mechanics*, 289: 351-378 (1995).

[20] Hornof, V.; Baig, F. U., Influence of interfacial reaction and mobility ratio on the displacement of oil in a Hele-Shaw cell. *Experiments in fluids*, 18: 448-453 (1995).

[21] Gland, N.; Pisarenko, D.; Kümpel, H. J., Controlling fingering instabilities in nonflat Hele-Shaw geometries. *Thermo-Hydro-Mechanical Coupling in Fractured Rock*, 160: 977-988 (2003).

[22] Brailovsky, I.; Babchin, A.; Frankel, M.; Sivashinsky, G., Fingering instability in water-oil displacement. *Transport in porous media*, 63: 363-380 (2006).

[23] Dias, E. O.; Parisio, F.; Miranda, J. A., Suppression of viscous fluid fingering: A piecewise-constant injection process. *Phys. Rev. E*, 82: 067301 (2010).

[24] Dias, E. O.; Miranda, J. A., Control of radial fingering patterns: A weakly nonlinear approach. *Phys. Rev. E*, 81: 016312 (2010).

[25] Reis, L. D.; Miranda, J. A., Controlling fingering instabilities in nonflat Hele-Shaw geometries. *Phys. Rev. E*, 84: 066313 (2011).

[26] Dias, E. O.; Alvarez-Lacalle, E.; Carvalho, M. S.; Miranda, J. A., Minimization of viscous fluid fingering: a variational scheme for optimal flow rates. *Phys. Rev. Lett*, 109: 144502 (2012).

[27] Dias, E. O.; Miranda, J. A., Minimization of instabilities in growing interfaces: A variational approach. *Phys. Rev. E*, 88: 062404 (2013).

[28] Yuan, Q.; Azaiez, J., Cyclic time-dependent reactive flow displacements in porous media. *Chemical Engineering Science*, 109: 136-146 (2014).

[29] Yuan, Q.; Azaiez, J., Inertial effects in cyclic time-dependent displacement flows in homogeneous porous media. *The Canadian Journal of Chemical Engineering*, 93 (8): 1490-1499 (2015).

[30] Chen, C. Y.; Huang, Y. C.; Huang, Y. S.; Miranda, J. A., Enhanced mixing via alternating injection in radial Hele-Shaw flows. *Phys. Rev. E*, 92: 043008 (2015).

[31] Ahmadlouydarab, M.; Azaiez, J.; Chen, Z., Immiscible flow displacements with phase change in radial injection. *International Journal of Multiphase Flow*, 72: 73-82 (2015).

[32] Lins, T. F.; Azaiez, J., Flow instabilities of time-dependent injection schemes in immiscible displacements. *The Canadian Journal of Chemical Engineering*, 94 (11): 2061-2071 (2016).

[33] Lins, T. F.; Azaiez, J., Resonance-like dynamics in radial cyclic injection flows of immiscible fluids in homogeneous porous media. *Journal of Fluid Mechanics*, 819: 713-729 (2017).

[34] Lins, T. F.; Azaiez, J., Dynamic control of droplets and pockets formation in homogeneous porous media immiscible displacements. *Physics of Fluids*, 30: 032105 (2018).

[35] Surguchev, L.; Koundin, A.; Melberg, O.; Rolfsvag, T. A.; Menard, W. P., Cyclic water injection: improved oil recovery at zero cost. *Petroleum Geoscience*, 8 (1): 89-95 (2002).

[36] Li, S.; Lowengrub, J. S.; Fontana, J.; Palffy-Muhoray, P., Control of viscous fingering patterns in a radial Hele-Shaw cell. *Phys. Rev. Lett*, 102: 174501 (2009).

[37] Huang, Y. S.; Chen, C. Y., A numerical study on radial Hele-Shaw flow: influence of fluid miscibility and injection scheme. *Computational Mechanics*, 55: 407–420 (2015).

[38] Leshchiner, A.; Thrasher, M.; Mineev-Weinstein, M. B.; Swinney, H. L., Harmonic moment dynamics in Laplacian growth. *Phys. Rev. E*, 81: 016206 (2010).

[39] Elgahawy, Y., & Azaiez, J. (2020). Rayleigh–Taylor instability in porous media under sinusoidal time-dependent flow displacements. *AIP Advances*, *10*(7).

[40] Yuan, Q., Zhou, X., Wang, J., Zeng, F., Knorr, K. D., & Imran, M. (2019). Control of viscous fingering and mixing in miscible displacements with time-dependent rates. *AIChE Journal*, *65(1)*, *360-371*.